Synthesis and study of nanostructures based on asbestos, silica and borate glasses with the inclusion of 2-methylbenzimidazole in a system of nanotubes or nanopores

© E.V. Balashova, A.A. Levin, S.I. Pavlov, V.Yu. Davydov, A.N. Smirnov, A.V. Fokin, A.N. Starukhin, D.A. Kurdyukov, D.A. Eurov, B.B. Krichevtsov

Ioffe Institute,
St. Petersburg, Russia

E-mail: balashova@mail.ioffe.ru

Received May 11, 2023
Revised July 31, 2023
Accepted October 30, 2023

The results of a study of organic nanostructures prepared by introducing heterocyclic 2-methylbenzimidazole (MBI) molecules into nanopores of borosilicate glasses and nanotubes of mesoporous silica and chrysotile asbestos are presented. Nanostructures were studied using X-ray diffractometry, infrared absorption spectroscopy, photoluminescence and dielectric spectroscopy.

Keywords: organic nanostructures, XRD, FTIR, photoluminescence, dielectric properties.

DOI: 10.61011/PSS.2023.12.57647.4993k

Nanosystems formed by introducing a filler with magnetic, ferroelectric or superconducting properties into matrices whose structure has nanoscale voids (nanopores or nanotubes), are of great interest. Examples of such matrices include nanoporous borosilicate glasses, chrysotile asbestos (ChA), and mesoporous silica [1]. The nanosystems formed by organic fillers, which can have ferroelectric and piezoelectric properties of particular interest [2]. The presented paper relates to the study of organic nanostructures obtained by introducing heterocyclic molecules of 2-methylbenzimidazole $C_8H_8N_2$ (MBI) into porous glasses, ChA and silica. MBI crystals have ferroelectric properties above room temperature [3]. Since the pores of glasses, silica and ChA tubes have nanometer dimensions, there is interest in study the formation of MBI nanocrystallites in such matrices, their lattice cell parameters, microstructure characteristics, as well as infrared absorption spectra, photoluminescence (PL) and dielectric properties.

The introduction of MBI molecules into the pores of glasses with pore sizes ~ 7 nm (MBI7) and ChA nanotubes (MBI_{ChA}) was carried out from the melt or gas phase of MBI. Spherical silica particles were synthesized by hydrolysis of tetraethoxysilane in an alcohol-water-ammonia medium containing a pore-forming substance — cetyltrimethylammonium bromide [4]. The average size of the resulting particles was 510 ± 30 nm, pore size 3.1 ± 0.2 nm. (insert in Figure 1, *c*). MBI was introduced into the silica pores by capillary impregnation from alcohol solution. Samples MBI7 and MBI_{ChA} were plates with dimensions $\sim 5 \times 5 \times 0.5\,mm^3$, and MBI_{silica} — a powder of mesoporous silicon particles. The pores in MBI7 are arranged randomly, and the nanotubes MBI_{ChA} are oriented parallel to the surface of the plate. The diameters of pores and nanotubes were estimated by mercury porosimetry and gas adsorption methods. The degree of filling of the pores (nanotubes) of the samples was determined by the weight change of the matrix and amounted to $\sim 80\%$ in the case of MBI_{ChA} and MBI7, and $\sim 20\%$ in the case of MBI_{silica}.

The obtained samples were measured by X-ray diffractometry (XRD) using D2 Phaser diffractometer (Bruker AXS, Germany). Links to programs (Celsiz, SizeCr, TOPAS (version 5), RietEsd) used to determine unit cell parameters, sizes of regions of coherent scattering of X-rays (crystallites) and microdeformations in them by graphical methods Crystallite size — Microdeformation (SSP) and Williamson-Hall (WHP), as well as for Rietveld quantitative analysis, are given in [5].

To measure infrared absorption spectra (FTIR) in the range $\nu = 650-5000\,cm^{-1}$, IRPrestige-21 IR-Fourier spectrophotometer (Shimadzu, Japan) was used. Photoluminescence (PL) measurements were carried out on LabRAM HREvo UV-VIS-NIR-Open spectrometer (Horiba, Lille, France). To excite luminescence the laser radiation with wavelengths $\lambda = 325$ nm ($E_{photon} = 3.814$ eV) or 405 nm ($E_{photon} = 3.061$ eV) was used. Capacity and dielectric loss measurements were carried out in the frequency range $(25-1 \cdot 10^6)$ Hz using E7-20 LCR meter (MNIPI, Minsk, Belarus).

1. MBI in chrysotile asbestos and silica

Fibers of ChA ($Mg_3(Si_2O_5)(OH)_4$) form a hexagonal close packing. The tube walls consist of approximately 20 double tape layers, which are twisted into tubes with an internal diameter of $\sim 2-8$ nm and an outer diameter of $\sim 20-40$ nm [1]. Figure 1, *a* shows X-ray diffraction pattern MBI_{ChA} measured from the largest face of the plate when X-ray scattering occurs perpendicular to the nanotubes. X-ray phase analysis showed that all observed

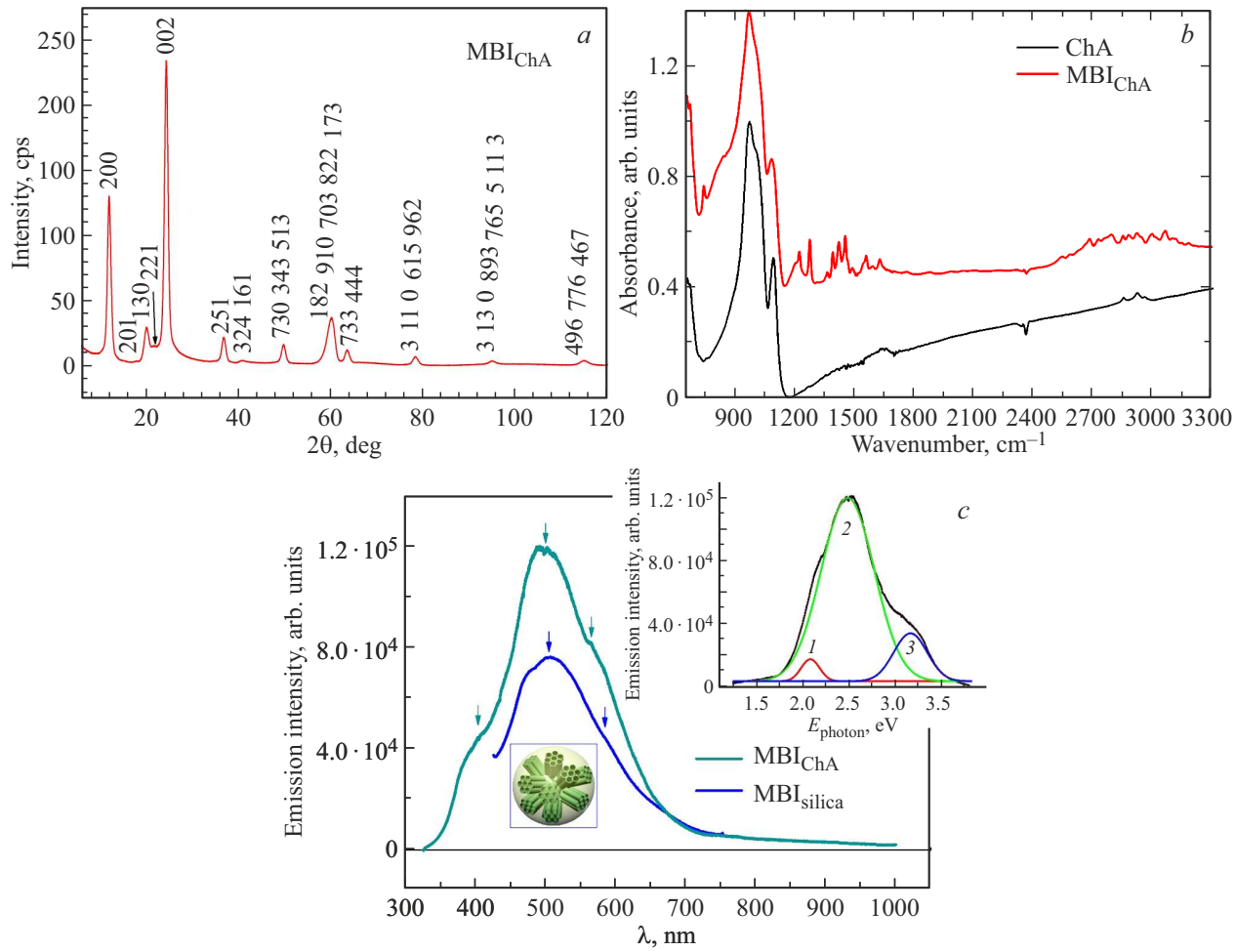

Figure 1. (*a*) Diffraction pattern of the nanostructure MBI_{ChA}. The Miller indices *hkl* of the observed reflexes of the MBI crystalline phase are indicated. (*b*) IR absorption spectra of asbestos sample and MBI_{ChA}. For clarity, the spectra are shifted vertically. (*c*) PL MBI spectra in ChA (MBI_{ChA}) when excited by light with $\lambda_{exc} = 325$ nm and in silica (MBI_{silica}, $\lambda_{exc} = 405$ nm). The insert on the left shows a diagram of the arrangement of nanopores in silica microparticle; the insert on the right shows the decomposition of the spectrum MBI_{ChA} into three Gaussian components.

reflexes belong to the MBI phase ($a = 13.950(13)$ Å, $c = 7.145(11)$ Å according to calculations using the Celsiz program), no ChA reflexes were observed. Estimating the crystallite sizes by the half-widths (FWHM) of reflexes with Bragg angles up to 38 degrees in the zero microdeformation approximation ($\varepsilon_s = 0$) using the Scherrer equation (with the coefficient $K_{Sherrer} = 0.94$), gives the average crystallite size $D \sim 9.1(9)$ nm, which satisfactorily corresponds to the internal diameter of nanotubes ChA.

MBI presence in the structure MBI_{ChA} is confirmed by FTIR spectra (Figure 1, *b*, Table 1). In addition to the ChA peaks in the IR spectrum MBI_{ChA}, peaks are observed in the ranges 1150–1750 cm^{-1} and 2500–3200 cm^{-1} associated with vibrations in MBI molecules [6].

The photoluminescence of „pure“ ChA is very weak. The introduction of MBI into ChA is accompanied by the appearance of bright luminescence (Figure 1, *c*). The main contribution to the PL spectrum comes from bands with energies $E_{photon} = 2.08$, 2.48 and 3.16 eV. A similar structure is observed also in the emission spectrum of MBI introduced into nanopores of mesoporous silica (Figure 1, *c*). Note that there are no MBI reflexes in the XRD diffraction pattern of MBI_{silica}, since the resulting MBI crystallites are too small ($\lesssim 2$ nm). Under these conditions the optical spectroscopy data are significant: the observation in MBI_{silica} of PL spectrum similar to MBI_{ChA} proves the entry of MBI into the pores of mesoporous silica particles. Note that bands with similar energies were also observed in the PL spectra of crystals α- and γ-glycine, as well as triglycine sulfate doped with croconic acid [7,8]. Flat cyclic molecules of croconic acid (CA), $C_5O_5H_2$, entering the pores of crystals form hydrogen bonds of type O...H–O and O...H–N, which can cause the appearance of strong PL. Flat heterocyclic MBI molecules ($C_8H_8N_2$) have two nitrogen atoms in the imidazole ring. The hydroxyl groups present in ChA and mesoporous silica can also form with MBI hydrogen bonds of O...H–N type. Studying the influence of these hydrogen bonds on PL is of undoubted interest.

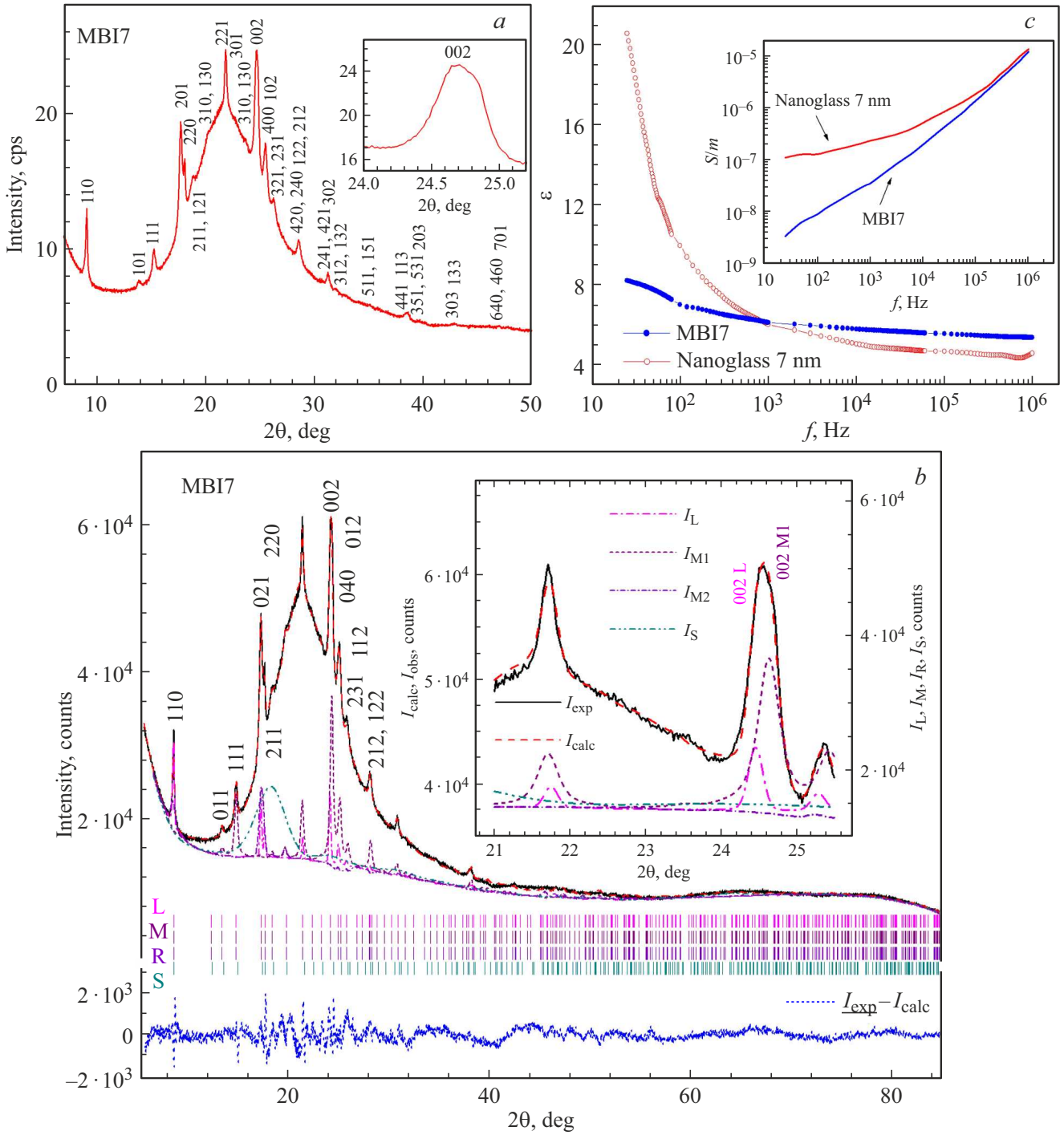

Figure 2. (*a*) X-ray diffraction pattern of sample MBI7. The Miller indices *hkl* of the observed X-ray reflexes are shown. The insert illustrates the broadening of the 002 reflex. (*b*) Results of Rietveld fitting of the MBI7 diffraction pattern within the framework of the four-phase model MBI (L (MBI_{large}), M1 (MBI_{ean1}), M2 (MBI_{mean2}) and S (MBI_{small})) with different crystallite sizes, characterized by slightly different lattice cell parameters and different directions of preferential orientation. The Miller indices *hkl* of selected observed X-ray reflexes are shown. The inset illustrates the contribution of different phases to the total observed reflection 002. (*c*) Frequency dependences of dielectric permittivity ε in a porous matrix of borate glass (nanoglass 7 nm) and in the porous matrix of glass with MBI inclusion (MBI7). The insert shows the frequency dependences of conductivity S/m for the same samples.

Table 1. Position of MBI absorption peaks in the FTIR spectra of the sample MBI_{ChA}. The second column shows the interpretation of MBI lines [6]. Abbreviations: Γ — out-of-plane bending, δ — in-plane bending, ν — stretching (stretching vibrations), M — methyl group.

ν, cm^1	Interpretation based on literature data [6]
1219	δCCH+νCN+νCC
1271	νCN+νCC+δCCH
1360	νCCH+νCN
1389	νCC+νCN+MδCH2
1418	MδCH2+δCCH
1448	δCCH+νCC
1485	MδCH2+ΓCCCN+δCCH
1555	νCN+νCC
1624	νCC+νCN

2. MBI in borosilicate glass

Figure 2, *a* shows the X-ray diffraction pattern of the MBI7 sample. X-ray diffraction analysis showed that all observed reflexes can be attributed to MBI (Figure 2, *a*). Analysis of reflex profiles indicates that the width of reflexes can vary greatly, with some reflexes even bifurcating. This fact indicates the presence in the samples of nanocrystallites belonging to the same crystalline phase (MBI), but having different sizes and characterized by slightly different unit cell parameters.

For sample MBI7, the experimental data are described in a four-phase model MBI (MBI_{large}, MBI_{mean1}, MBI_{mean2} and MBI_{small}) with different crystallite sizes and, accordingly, different characteristic values of FWHM reflexes of these phases. The results of Rietveld fitting (using the TOPAS program) of the MBI7 diffraction patterns are presented in Figure 2, *b* and in Table 2. MBI7 structure contains phases with crystallite sizes $D = 61(3)$ nm (MBI_{large}), $D = 28(1)$ nm (MBI_{mean1}) and $D = 17(1)$ nm (MBI_{mean2}). There is also phase MBI_{small} with crystallite sizes $D = 2.7(1)$ nm, smaller than the pore sizes ~ 7 nm. Taking this phase into account leads to a significant decrease in divergence factors (weight profile factor $R_{wp} = 1.64\%$ and weight profile factor with subtraction of the background contribution $cR_{wp} = 13.02\%$) compared to the model not considering MBI_{small} ($R_{wp} = 2.53\%$ and $cR_{wp} = 30.40\%$), which confirms the presence of phase MBI_{small}. The crystallite sizes obtained in the Rietveld fitting are in good agreement with the results obtained using the SizeCr programs and the graphical methods SSP and Williamson-Hall (WHP).

Thus, in the MBI7 system there is a very small amount (~ 0.8 wt.%) of crystallites of phase MBI_{large} ($D \sim 61$ nm).

Table 2. Results of Rietveld quantitative analysis (the atomic coordinates of the crystalline phases were not specified) of the MBI7 sample and agreement factors characterizing the quality of the fitting up (R_B, R_{wp}, R_p, cR_{wp} and cR_p)[a]

Crystalline Phase[b]	a, Å c, Å	D, nm ε_s, %[c]	D^{SSP}, nm[cd] ε_s^{SSP}, %[cd]	Wt, wt.% B_{iso}^{ovl}, $Å^{-2e}$	R_B, % r^f	R_{wp}, % R_p, % $m_{e.s.d.g}$	cR_{wp}, % cR_p, %
Model $MBI_{large} + MBI_{mean1} + MBI_{mean2} + MBI_{small}$							
MBI_{large}	13.943(9) 7.272(3)	61(3) 0.014(6)	57(5) 0.06(12)	0.80(2) 1.0(4)	0.47 1.24(3)	1.63 1.27	13.02 16.15
MBI_{mean1}	14.025(2) 7.221(1)	28.7(3) 0	31(3) 0	12.52(6) 4.3(6)	0.77 0.62(1)	5.83	
MBI_{mean2}	14.014(17) 7.190(12)	17(1) 0	18(4) 0	9.71(17) 3.9(5)	1.26 0.21(1)		
MBI_{small}	13.910(16) 7.176(34)	2.7(1) 0	– –	83.79(29) B_{iso}^{ov} MBI_{mean2}	0.27 0.10(1)		

Note: [a] Bragg agreement factor R_B, weight profile (R_{wp}) and profile (R_p) agreement factors and their analogues cR_{wp} and cR_p, corrected for background contribution.

[b] Space group of phases MBI — $P4_2/n$ (86). Parameters of lattice cell according to CCDC data, $a = 13.950(9)$ Å, $c = 7.192(3)$ Å (code CCDC 1199885). During the Rietveld quantitative analysis (with the Rietveld fitting of the X-ray diffraction pattern), the atomic coordinates were taken from CCDC 1199885 and not clarified.

[c] Microdeformation ε_s was recalculated as $\varepsilon_s = 2 \cdot e_0 \cdot 100\%$ from microdeformation parameter e_0, obtained using TOPAS.

[d] Values of sizes of average crystallites D^{SSP} and microdeformations ε_s^{SSP}, obtained by SSP method are shown. The WHP method produces similar values, but with larger estimated standard deviations (e.s.d.s.).

[e] Isotropic temperature factor of atoms, common to all atoms of the structure.

[f] March-Dollase parameter of preferred crystallite orientation along [001], [012], [241] and [211] for MBI_{large}, MBI_{mean1}, MBI_{mean2} and MBI_{small} respectively.

[g] e.s.d.s. shown in Table 2 in parentheses are corrected for underestimation due to serial correlations by multiplying e.s.d.s. obtained by refining the parameters during the Rietveld fitting process by the factor $m_{e.s.d.}$.

Two phases with average crystallite sizes ~ 28 nm (phase MBI_{mean1}) and ~ 17 nm (phase MBI_{mean2}) occupy in total ~ 15.41 wt.%. The largest volume ~ 83.79 wt.% is occupied by crystallites with dimensions ~ 2.7 nm (Table 2). MBI phases with sizes larger than the diameter of the glass pores are apparently formed in areas of the pores that run nonparallel to the surface of the sample MBI7.

Figure 2, *c* shows the dependences of the effective dielectric permittivity of borate glass without inclusion (nanoglass) and with inclusion of MBI (MBI7). The introduction of MBI results in increase in the effective dielectric permittivity at high frequencies due to the higher dielectric permittivity of MBI ($\varepsilon \cong 8-10$) compared to glass. However, at low frequencies, higher ε is observed in „pure“ nanostructures, without the inclusion of MBI. This may be due to the presence of various molecules adsorbed from the air in the nanopores. Frequency dependences of conductivity (insert in Figure 2, *c*) show that these molecules determine the direct current conductivity $\sigma \approx 8 \cdot 10^{-8}$ S/m. At the same time, the inclusion of MBI dielectric into nanopores significantly reduces the nanostructure conductivity at low frequencies. Frequency dependences of conductivity in the high-frequency region are usually described by exponential function $\sigma_{AC} \sim \omega^s (s \leq 1)$. For MBI nanostructures, the exponent $s \cong 0.92$ is observed. $s < 1$ decreasing may be associated with the manifestation of a specific mechanism of hopping conductivity [9] or with the manifestation of a size effect.

Unlike ChA-based samples, the introduction of MBI into porous glass does not lead to a strong increase in PL, as occurs in MBI_{ChA}. At the same excitation light intensity the PL intensity in MBI-filled nanoglass increases by approximately 2–3 times compared to pure glass.

Funding

X-ray diffraction studies were performed on the equipment of the Federal Common Use Center „Materials Science and Diagnostics in Advanced Technologies“ (Ioffe MFTI, St. Petersburg, Russia).

Conflict of interest

The authors declare that they have no conflict of interest.

References

[1] Yu.A. Kumzerov, S. Vakrushev. In: Encyclopedia of Nanoscience and Nanotechnology / Ed. H.S. Nalwa. American Scientific Publ. (2004). V. VII. P. 811–849. https://doi.org/10.1166/000000004323036991.
[2] D. Lombardo, L. Pasqua, S. Magazú. Materials **13**, 1048 (2020). https://doi.org/10.3390/ma13051048.
[3] S. Horiuchi, F. Kagawa, K. Hatahara, K. Kobayashi, R. Kumai, Y. Murakami, Y. Tokura. Nature Commun. **3**, 1308 (2012). https://doi.org/10.1038/ncomms2322.
[4] E.Yu. Trofimova, D.A. Kurdyukov, S.A. Yakovlev, D.A. Kirilenko, Yu.A. Kukushkina, A.V. Nashchekin, A.A. Sitnikova, M.A. Yagovkina, V.G. Golubev. Nanotechnology **24**, 155601 (2013). DOI: 10.1088/0957-4484/24/15/155601.
[5] E.V. Balashova, F.B. Svinarev, A.A. Zolotarev, A.A. Levin, P.N. Brunkov, V.Yu. Davydov, A.N. Smirnov, A.V. Redkov, G.A. Pankova, B.B. Krichevtsov. Crystals **9**, 573 (2019). DOI: 10.3390/cryst9110573.
[6] M.T. Güllüoglua, M. Özdurana, M. Kurt, S. Kalaichelvan, N. Sundaraganesan. Spectrochimica A **76**, 107 (2010). DOI: 10.1016/j.saa.2010.02.032.
[7] E. Balashova, A.A. Levin, V. Davydov, A. Smirnov, A. Starukhin, S. Pavlov, B. Krichevtsov, A. Zolotarev, H. Zhang, F. Li, H. Ke. Crystals **12**, *5*, 679 (2022). DOI: 10.3390/cryst12050679.
[8] E. Balashova, A.A. Levin, V. Davydov, A. Smirnov, A. Starukhin, S. Pavlov, B. Krichevtsov, A. Zolotarev, H. Zhang, F. Li, H. Ke. Crystals **12**, *10*, 1342 (2022). DOI: 10.3390/cryst12101342.
[9] G.E. Pike, Phys. Rev. B **6**, 1572 (1972). DOI: 10.1103/PhysRevB.6.1572

Translated by I.Mazurov